INCREASING THE EXTERNAL DAMPING OF A FLEXIBLE ROTOR BY PERIODIC CONTROL

F. Dohnal
Institute for Structural Dynamics
Technische Universität Darmstadt
Petersenstraße 30
64287 Darmstadt, Germany
Tel.: +496151166704, Fax: +496151163668
Email: dohnal@sdy.tu-darmstadt.de

Abstract
The influence of a periodic open-loop control operated in parallel to an existing closed-loop PID control is investigated on a rotor system supported by two radial active magnetic bearings. The transient behaviour of the rotor is studied numerically and first experimental results are shown to demonstrate the applicability of the method. It is highlighted that by tuning the periodic control properly it is possible to amplify artificially the external damping of the rotor system. This concept allows increasing the total external damping well beyond the stability margin of the closed-loop control cycle.

1 Introduction

Systems of differential equations with periodic coefficients, also termed parametrically excited systems, have been the focus of scientific research for a long time. The frequency of the parameter change is prescribed explicitly as a function of time and is independent of the motion of the system. Classical examples are a periodically moving pivot point of a pendulum or a rotating shaft with a nonsymmetric cross-section. Parametrically excited systems and structures have been studied extensively in the past because of the somehow unexpected dynamic phenomena that occur in such systems. A parametrically excited system may exhibit a destabilising parametric resonance if the variation frequency is close to [10]

$$\nu_0 = \frac{|\omega_k \mp \omega_l|}{n}, \qquad k = 1, 2, \ldots . \qquad (1)$$

Herein ω_i denotes the ith natural frequency of the underlying undamped system and n is a natural number. Several publications deal with a single or coupled differential equations having time-periodic coefficients [1, 7]. The main focus there was to investigate the destabilising effect of parametric excitation, i.e. the instability boundary curves in the domain of system parameters. The non-resonant cases were not considered to be relevant for applications. The mechanism of damping by parametric excitation, as investigated here, is based on the coupling of vibration modes which leads to an artificial increase of the overall damping in the system. A specific control frequency at which the system vibrations are reduced is termed as a parametric *anti*-resonance frequency. The main theoretical contributions with respect to parametric anti-resonances in this context can be found in [8, 2, 4].

Very few studies have been undertaken to verify the existence of parametric anti-resonances experimentally. Mainly discrete 2DOF systems of an artificial nature have been investigated so far. The main motivation of the present study is to prove experimentally that the concept of damping by parametric excitation is applicable for damping the low-frequency modes of a complex, flexible rotor system.

A parametric excitation can be introduced in the system in a simple open-loop manner, since the stiffness parameter in focus needs to be varied at a well-defined, fixed frequency and fixed amplitude. The present paper examines this open-loop strategy to increase the effective damping of a rotor system based on preliminary theoretical investigations [9, 3]. Therein, it was shown theoretically that a periodic change in the bearing stiffness is capable of increasing the critical speed of a simple Jeffcott rotor under the influence of a destabilising self-excitation. Now, this approach is used to enhance the damping of an already stable system and realised experimentally for a complex flexible rotor system supported by active magnetic bearings.

First, the model equations of a flexible rotor system with multiple rigid disks attached to its shaft are stated. Then, a numerical prediction is given for the regions where damping by parametric excitation is effective. Finally, first experimental results are compared to the theoretical predictions. This work summarises the contribution [5].

2 Lateral vibrations of a flexible rotor with multiple rigid disks

The mechanical model of the rotor system under consideration is shown in Fig. 1. A slender, flexible rotor shaft is rotating at a constant rotational speed Ω provided by a driving motor. The shaft is assumed to be torsionally rigid and isotropic. Five rigid, unbalanced disks are attached to the shaft, three disks (D1, D2, D3) and two bearing studs (AMB1, AMB2). The shaft is supported by two active magnetic bearings. The actual stud position is measured and fed back to decentralised PID controller for position control. The total length of the shaft is 680 mm.

The flexible, continuous shaft is discretised using a single finite beam element between two disks, see e.g. [6]. Rigid disks with mass and moment of inertia are attached at discrete positions along the shaft. Their symmetry axis is aligned with the central rotary axis leading to a diagonal mass matrixThe element matrices are assembled to the global stiffness and mass matrices of the continuous shaft, $\mathbf{C}_b^{z/y}$ and $\mathbf{M}_b^{z/y}$, and the global mass matrix $\mathbf{M}_r$ of the rigid disks, all with respect to the global coordinate vector of lateral displacements and inclinations.

The electromagnetic force generated by the active magnetic bearing (AMB) depends on its geometry parameters (cross-section of the pole shoes, size of the air gap) and its electromagnetic properties (number of turns, permeability) and is a strongly non-linear function of these parameters. In practice, however, the resulting force can be linearised close to a certain operation point as

$$F_m^{lin} = k_i i_c - k_s r, \tag{2}$$

assuming a high bias current for pre-magnetisation and small control current i_c and rotor deflection r. Herein, k_i is the current-force constant and $-k_s$ the negative bearing stiffness. Cross-coupling parameters are neglected.

The most widely used control concept for an AMB is a PID controller. The proportional (k_P) and the derivative actions (k_D) constitute the stiffness and damping characteristics of the bearing while the integral action (k_I) assures that the resulting rotor deflection r keeps track with a predefined setpoint,

$$i_c = k_P\, r + k_D\, \dot{r} + k_I \int r\, dt. \tag{3}$$

Inserting into eq. (2) leads to

$$F_m^{lin} = c_m r + d_m \dot{r} + k_i k_I \int r\, dt, \tag{4}$$

with the active stiffness and active damping coefficients

$$c_m = k_i k_P - k_s, \qquad d_m = k_i k_D. \tag{5}$$

Adjusting the control parameters k_P and k_D determines the dynamic properties of the AMB. Both AMBs are assumed to be isotropic. With the mechanical properties in eq. (5), the stiffness and damping matrices ($\mathbf{C}_m$ and $\mathbf{D}_m$) have diagonal form with entries at the location of the AMBs.

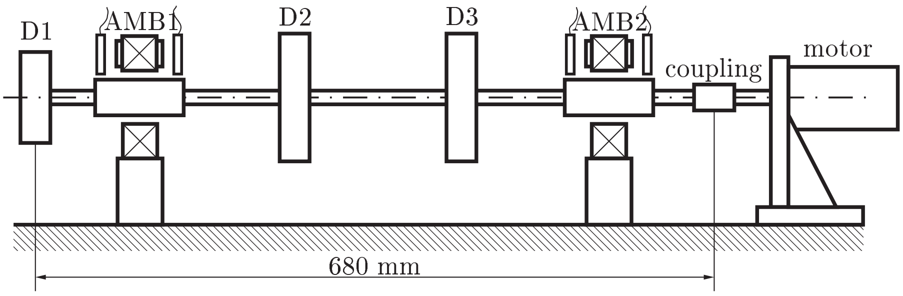

Fig. 1: Flexible rotor with multiple disks and electromagnetic supports.

rotor	bending stiffness of rotor shaft	41.4 N/m
	mass per unit length of shaft	0.4 kg/m
	total length of rotor and shaft diameter	680 mm, 8 mm
	mass and axial moment of inertia of disk D1	0.78 kg, $0.4 \cdot 10^{-3}$ kg m^2
	mass and axial moment of inertia of disk D2 and D3	1.20 kg, $1.4 \cdot 10^{-3}$ kg m^2
	mass of studs in AMB1 and AMB2	0.88 kg
AMBs	number of electromagnets	4 in each bearing
	magnetic bearing constant	$3.64 \cdot 10^{-6}$ Vsm/A
	current-force constant k_i	42.1 N/A
	bearing stiffness k_s	$1.052 \cdot 10^5$ N/m
	controller sampling frequency	8 kHz
	radial clearance	0.80 mm

Table 1: Details of rotor system in Fig. 1.

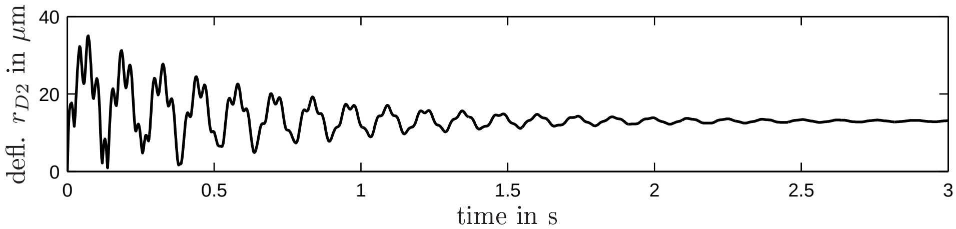

Fig. 2: Rotor deflection of disk D2 under the action of unbalance forces for $\varepsilon = 0$.

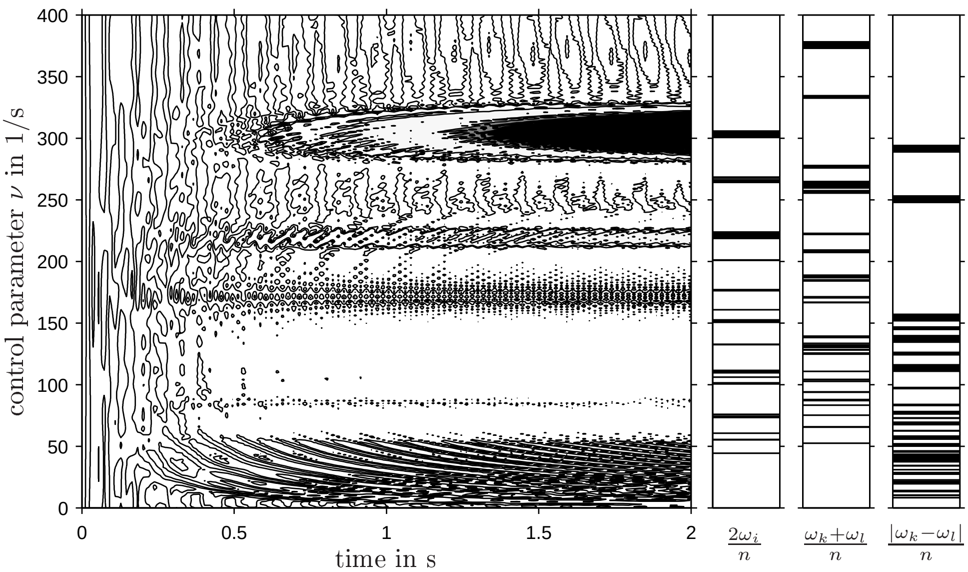

Fig. 3: Time histories of r_{D2} in dependency of the control parameter ν at $\varepsilon = 0.30$.

The rotor system is excited by unbalance forces $\mathbf{f}_z$, $\mathbf{f}_y$ originating from eccentricities of the five rigid disks (including the bearing studs).

Together with the electromagnetic actions, the equations of motion of the rotor system with respect to the global coordinate vector $\mathbf{q} = [\mathbf{q}^{z,T}, \mathbf{q}^{y,T}]^T$ become

$$\mathbf{M}\,\ddot{\mathbf{q}} + \mathbf{D}\,\dot{\mathbf{q}} + \mathbf{C}\,\mathbf{q} = \mathbf{f} \qquad (6)$$

with the assembled coefficient matrices and the global force vector

$$\mathbf{M} = \begin{bmatrix} \mathbf{M}_b^z + \mathbf{M}_r & \mathbf{0} \\ \mathbf{0} & \mathbf{M}_b^y + \mathbf{M}_r \end{bmatrix},$$
$$\mathbf{D} = \begin{bmatrix} \mathbf{D}_m & -\Omega\mathbf{G}_r \\ \Omega\mathbf{G}_r & \mathbf{D}_m \end{bmatrix}, \quad \mathbf{f} = \begin{bmatrix} \mathbf{f}^z \\ \mathbf{f}^y \end{bmatrix},$$
$$\mathbf{C} = \begin{bmatrix} \mathbf{C}_b^z + \mathbf{C}_m & \mathbf{0} \\ \mathbf{0} & \mathbf{C}_b^y + \mathbf{C}_m \end{bmatrix}. \qquad (7)$$

The only source of damping is the control strategy in the AMBs. The lateral vibrations in y- and z-directions are coupled by gyroscopic effects of the rigid disks. The operational deflection of the present rotor is assumed to be sufficiently small such that rotor-stator contacts with safety bearings are excluded and the linearisation of the electromagnetic force in eq. (2) remains valid.

A time-periodic stiffness variation in the rotor system is realised in the AMBs by introducing a time-dependent proportional action $k_P(t)$ in the PID controllers. This control parameter is changed periodically for both AMBs simultaneously according to

$$k_P(t) = k_P\,(1 + \varepsilon \sin \nu t) \qquad (8)$$

resulting in the global time-periodic stiffness matrix

$$\mathbf{C}(t) = \mathbf{C}_0 + \varepsilon\,\mathbf{C}_t \sin \nu t, \qquad (9)$$

where $\mathbf{C}_0$, $\mathbf{C}_t$ are time-independent coefficient matrices.

Numerical study

The flexible rotor system in Fig. 1 is examined for a fixed set of system parameters listed in Table 1 for different values of the amplitude ε and the control frequency ν of the time-periodicity introduced in eq. (8). The equations of motion in eq. (6) are solved by direct numerical integration. Initially, the rotor shaft in Fig. 1 rests at the centre position $\mathbf{q} = \mathbf{0}$. Since unbalance forces $\mathbf{f}$ acts on the rotor system, the rotor shaft is deflected from this initial condition to a new deflection that rotates with the rotor speed Ω. The transition between these two states is described by free vibrations. A sample time history for the radial deflection of the disk D2

$$|r_{D2}| = \sqrt{y_{D2}^2 + z_{D2}^2} \qquad (10)$$

at constant, nominal AMB characteristics ($\varepsilon = 0$ in eq. (8)) and a constant rotor speed of $\Omega = 60$ 1/s is shown in Fig. 2. The same features are observed for the time histories at the other disk positions and are therefore omitted.

The first two natural frequencies obtained from an eigenvalue analysis of the undamped system in eq. (6) at rest together with the resulting parametric resonance and anti-resonance frequencies are listed in Table 2. Evaluating the analytical predictions in [2] reveals that for the present system only the parametric excitation frequencies of difference type in eq. (1), $|\omega_k - \omega_l|/n$, correspond to parametric anti-resonance frequencies at which an increase of effective damping is achievable. Within the present investigation, the influence of gyroscopic effects on the first four natural frequencies is below 4%. Note that the time history in Fig. 2 describes the radial deflection of a disk in a coordinate system that is fixed to the disk. Consequently, the observed frequency components correspond to the speed-dependent natural frequencies $\omega_i[\Omega]$ that are modulated by the rotor speed Ω. The lowest frequency component in Fig. 2 becomes $|\Omega - \omega_1|/2\pi \approx 8$ Hz.

Now, the periodic open-loop control in the AMBs is switched on following the control law in eq. (8). The vibration behaviour

natural frequencies	
$\omega_1 = 110.6$ 1/s,	$\omega_2 = 151.6$ 1/s
main parametric resonance frequencies	
$2\omega_1 = 221.2$ 1/s,	$2\omega_2 = 303.2$ 1/s,
$\omega_1 + \omega_2 = 262.2$ 1/s	
main parametric anti-resonance frequency	
$\lvert\omega_1 - \omega_2\rvert = 41.0$ 1/s	

Table 2: First frequencies at rest, $\Omega = 0$.

ν in 1/s	ε	log. decr.
113	0.00	1.9
113	0.15	2.5
113	0.30	3.9
113	0.45	4.6

Table 3: Logarithmic decrement at the optimum control parameter $\nu = |\omega_2 - \omega_3|$.

is investigated at a control amplitude of $\varepsilon = 0.30$ and a fixed control frequency ν in the range between 0 and 400 1/s. Numerical integration of the equations of motion in eq. (6) at $\nu = 0$ 1/s results in the time history already shown in Fig. 2. All time histories in the frequency range of interest are summarised in the contour plot in Fig. 3. Light areas depict low values and dark areas high values of the disk deflection $|r_{D2}|$. Additionally, frequency lines of the frequencies ν_0 defined in eq. (1) are plotted for the orders $n = 1$ up to $n = 5$ on the right hand side of the figure. Their line thickness is scaled by the order n. The frequencies listed in Table 2 are of order $n = 1$ and are plotted as lines with the largest thickness. All possible frequency combinations ν_0 are divided into three groups corresponding to the three block on the right hand side of the figure: the two groups $2\omega_i/n$ and $(\omega_k + \omega_l)/n$ that correspond to destabilising parametric excitation frequencies, and the group $|\omega_k - \omega_l|/n$ which corresponds to stabilising parametric frequencies. These frequency lines help encoding the complex distribution of the time series. At each of these frequencies a dense frequency interval exist within which the system vibrations are either excited or damped. If these frequency intervals overlap, it depends which effect dominates. In general, the destabilising effect at frequencies $2\omega_i/n$ dominates the effects acting at frequencies $|\omega_k \mp \omega_l|/n$.

Destabilising effects, a decrease in effective damping, are found where the control parameter ν is in the vicinity of the frequencies 49 1/s, 172 1/s, 221 1/s and 300 1/s. The corresponding parametric resonance frequencies can be identified by comparison with the frequency lines on the right hand side, e.g. the shaded area at 221 1/s corresponds to the frequency $2\omega_1 = 221.2$ 1/s. Indentations in the distribution towards lower time values in Fig. 3 give hints of an increase in effective damping. The main stabilising control frequency is found to be close to $\nu = |\omega_2 - \omega_3| = 113.4$ 1/s. This is the optimum control frequency to be chosen for the proposed open-loop control in eq. (8) for this specific rotor system.

The corresponding time histories of the deflection r_{D2} of disk 2 at the optimum control frequency $\nu = |\omega_2 - \omega_3|$ is shown in Figs. 4. The time history of the rotor system for switched off open-loop control ($\varepsilon = 0$) was presented in Fig. 2. Introducing the open-loop control in eq. (8) at a moderate control amplitude of $\varepsilon = 0.30$, increases the effective system damping slightly, see Fig. 4. Evaluating the logarithmic decrement of these time histories gives a good measure of the effective damping present in the rotor system. The determined values are summarised in Table 3. Hence, for the present system configuration the effective damping can be enhanced, or amplified, by a factor of 2.4.

It has to be highlighted that that the proposed open-loop control method works only if a certain level of the control amplitude ε is exceeded. Upon exceeding this value, an additional artificial damping is acting in the rotor system which increases the overall system damping. The drawback of the open-loop method applied to this example system is that although the transient vibration can be reduced significantly,

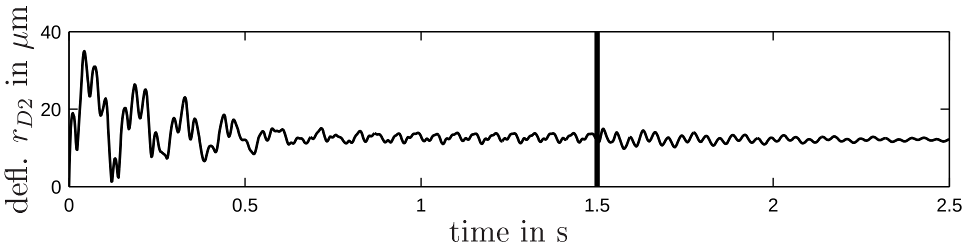

Fig. 4: Time history at optimal controller parameters $\nu = |\omega_2 - \omega_3|$ and $\varepsilon = 0.30$.

a certain level of oscillations remains at the final state due to the persistent alteration of the bearing stiffness. These oscillation increase for higher values of the controller amplitude. It depends on the application whether these oscillations interfere with the desired operation task or the artificial increase in damping can be justified. A proper countermeasure could be a simple on/off logic that activates the open-loop control on demand only, e.g. when the radial deflection exceeds a predefined limit. The effect of a simple on/off switch is shown in Fig. 4 where the proposed open-loop control is switched off at 1.5 s. Hence, the artificially increased system damping is switched back to its initial value and the rotor vibrations decrease with the lower initial system damping induced by the inherent active damping in the AMBs. A soft on/off switching is suggested to avoid sudden changes in the stiffness characteristics leading to small but impact-like excitation.

Experiment

In this section experimental results are presented that underline the theoretical findings from above. Figure 6 shows the experimental realisation of the system introduced in Fig. 1 and Table 1. The actual position of the rotor shaft is measured by inductive sensors (two for each radial direction y and z). These signals are processed by the real-time controller hardware dSpace, which implements the decentralised PID controllers in eq. (3) to regulate the currents provided to each of the electromagnets. In parallel to this PID control, an open-loop control of the proportional action is implemented according to eq. (8), which realises a periodic change in the active bearing stiffness.

At the sample rotor speed of 600 rpm (below the first critical speed), the rotor is levitated in the AMBs by the PID controllers, while the proportional action k_P is open-loop controlled at the theoretically predicted optimum control frequency $\nu = |\omega_2 - \omega_3| = 113.4$ 1/s. At the time of 8 s the system is excited by adding an impulse-like current to the controller current. Time histories for different values of the control amplitude ε are shown in Fig. 6. For the system without open-loop control ($\varepsilon = 0$), the system response decays with an effective logarithmic decrement of 0.8. Activating the open-loop control at the optimum frequency enhances the system damping artificially which results in increased logarithmic decrements. A value of 1.6 is achieved for the logarithmic decrement at a control amplitude of $\varepsilon = 0.15$ and a value of 3.7 (which lies well beyond the stability border of the PID control of 1.2) at $\varepsilon = 0.30$. Higher control amplitudes are not possible with the present set-up of the rotor test rig.

Without the proposed open-loop control ($\varepsilon = 0$), the system damping can be increased simply by the active damping d_m in eq. (5) introduced by the PID controllers, too. However, this increase is lim-

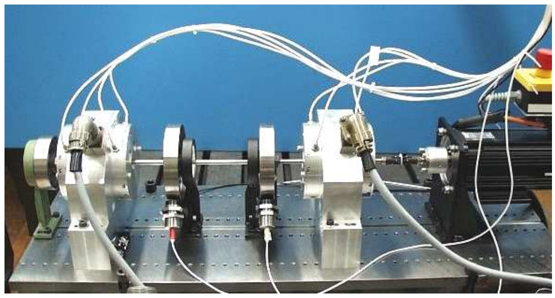

Fig. 5: Flexible rotor with multiple disks supported by two magnetic bearings.

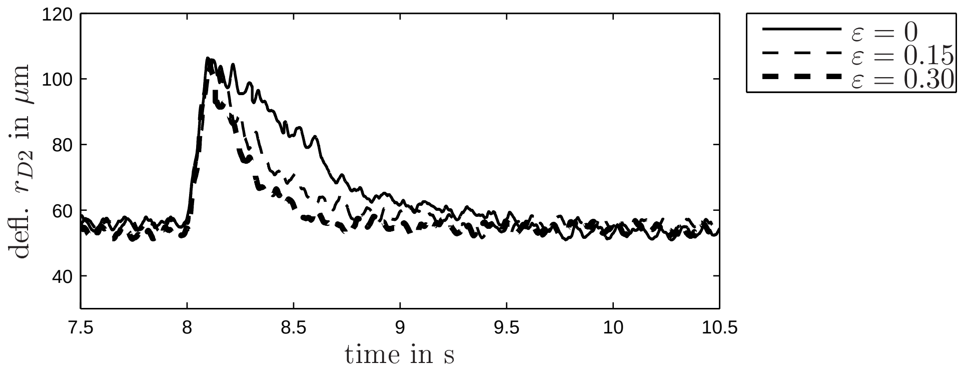

Fig. 6: Measured time histories at the optimal controller parameter $\nu = |\omega_2 - \omega_3|$.

ited by the level of measurement noise in the control loop and its amplification by the derivative action k_D. Starting from optimum PID controllers in the nominal system, k_D can be amplified maximally by a factor of 1.7. Introducing the proposed open-loop control at the control parameters $\varepsilon = 0.3$ and $\nu = |\omega_2 - \omega_3|$, allows an increase in effective system damping well above this factor. The maximum amplification factor for the effective damping that is achievable experimentally is 4.6 which lies well above the limit realisable by conventional active damping.

Summary

In this study new findings on damping by parametric excitation are presented. A flexible rotor system is analysed having support bearings with time-periodic, open-loop control of the stiffness coefficients. It is verified theoretically and demonstrated experimentally that the proposed open-loop control method is capable to increase the overall damping of a flexible rotor system. The open-loop method possesses several advantages. First, introducing a periodic change in the bearing stiffness works as an open-loop system with no feedback control necessary. Secondly, the control method can be applied in parallel with existent methods, since it affects mainly the free vibrations of a system. Finally, in the present system, the proposed control method is capable of increasing the effective damping well above the PID-stability margin.

References

[1] Bolotin, V.V., Dynamic stability of elastic systems, Holden-Day, 1964.

[2] Dohnal, F., Damping by parametric stiffness excitation: resonance and anti-resonance, Journal of Vibration and Control 14, 2008.

[3] Dohnal, F. and Mace B.R., Damping of a flexible rotor by time-periodic stiffness and damping variation, Proceedings of the 9th International Conference in Vibrations in Rotating Machinery, Oxford, UK, 2008.

[4] Dohnal, F., Damping of mechanical vibrations by parametric excitation: parametric resonance and anti-resonance, Südwestdeutscher Verlag, 2009.

[5] Dohnal, F., Markert, R., Enhancement of external damping of a flexible rotor in active magnetic bearings by time-periodic stiffness variation, Journal of System Design and Dynamics 5, 2011, pp. 856–865.

[6] Gèrardin, M. and Rixen, D., Mechanical vibrations – Theory and application to structural dynamics, Wiley, 1994.

[7] Nayfeh, A.H. and Mook, D.T., Nonlinear Oscillations, John Wiley and Sons, 1995.

[8] Tondl, A., To the problem of quenching self-excited vibrations, Acta Technica CSAV 43, Institute of Electrical Engineering, Academy of Science Czech Republic, 1998.

[9] Tondl, A., Self-excited vibration quenching in a rotor system by means of parametric excitation, Acta Technica CSAV 45, Institute of Electrical Engineering, Academy of Science Czech Republic, 2000.

[10] Yakubovich, V.A. and Staryhinskii, V.M., Linear differential equations with periodic coefficients, 1 and 2, Wiley, 1975.